Materials Letters 93 (2013) 56–59

Contents lists available at SciVerse ScienceDirect

Materials Letters

journal homepage: www.elsevier.com/locate/matlet

Synthesis and characterization of ball-in-ball CuSCN hollow architecture

Bo Chai *, Min Wang, Zhan Wang, Yourong Wang, Yuchan Zhu

School of Chemical and Environmental Engineering, Wuhan Polytechnic University, Wuhan 430023, PR China

ARTICLE INFO

Article history:
Received 5 September 2012
Accepted 18 October 2012
Available online 23 November 2012

Keywords:
CuSCN
Ball-in-ball
Poly(vinylpyrrolidone)
Solution method

ABSTRACT

Ball-in-ball CuSCN hollow architecture is successfully synthesized by a facile one-pot aqueous solution method in the presence of poly(vinylpyrrolidone) at room temperature. The as-synthesized products are characterized by X-ray diffraction (XRD), field emission scanning electron microscopy (FESEM), high-resolution transmission electron microscopy (HRTEM), X-ray photoelectron spectroscopy (XPS), UV–vis diffuse reflectance absorption spectra (DRS) and nitrogen adsorption–desorption measurement. A possible formation mechanism for CuSCN hollow spheres by the difference of solubility products (K_{sp}) of CuBr and CuSCN or chemical self-transformation is proposed based on the experimental observations. The band gap energy of hollow CuSCN sphere is estimated to be 3.77 eV based on the results of optical measurement. The BET specific surface area of ball-in-ball CuSCN hollow architecture is calculated to be 30.5 m^2/g and it has a bimodal mesoporous structure from nitrogen adsorption–desorption investigation.

1. Introduction

Usually, the particle sizes, shape and dimensionality strongly affect the properties of materials. Nanostructured materials with hollow structure have attracted considerable interest in the past few decades owing to their uniform size, low density, large surface area, and wide range of potential applications [1–4]. Conventional methods on the formation of hollow spheres usually require removable hard or soft templates, to direct the formation of inorganic nanoparticles on their surfaces *via* adsorption or chemical reactions [5,6]. Recently, Yu and coworkers have prepared the CuS/ZnS nanocomposite hollow spheres, CuO/Cu_2O hollow microspheres and TiO_2 hollow spheres by sacrificial templates method and chemically induced self-transformation process [7–13]. CuSCN, as a wide band gap (~3.7 eV) and p-type semiconductor has recently found wide application as a solid hole-transporting electrolyte in dye-sensitized and other nanostructured solar cells [14–18]. Several methods have reported the synthesis of CuSCN with different morphologies [19–22]. Yang et al. have prepared porous CuSCN spheres by a sol–gel technique at lower temperature [19]. Li et al. have synthesized flower-like CuSCN through hydrothermal route [20]. Xu and Xue have fabricated the upended taper-shaped CuSCN arrays on a copper substrate using a simple solution method at room temperature [21]. However, it remains a challenge to achieve the facile synthesis of CuSCN with hollow structure. Herein, we report a facile one-pot aqueous solution route to synthesis of ball-in-ball CuSCN hollow architecture in presence of poly(vinylpyrrolidone) (PVP). In addition, the BET surface area, optical property and band gap of the as-prepared sample are evaluated.

2. Experimental

Material preparation: All chemicals are analytical grade and used as received without further purification. In a typical procedure, an aqueous solution was first prepared by mixing 150 mL of water, 0.06 g poly(vinylpyrrolidone) (PVP, K30), and 4 mL of $CuBr_2$ solution (0.1 M). Then 10 mL of ascorbic acid solution (0.1 M) was added to the solution, and the mixture was stirred for 10 min and became turbid shortly, indicating the formation of CuBr particles. Following, 8 mL of KSCN solution (0.1 M) was added to the above turbid precursor solution under stirring, and the resulting solution was then kept for 30 min at room temperature without stirring. The resultant CuSCN products were filtered and washed with distilled water and absolute ethanol for several times, and then dried in vacuum at 80 °C for 4 h.

Material characterization: The products were characterized by X-ray powder diffraction (XRD) patterns using Bruker D8 Advance X-ray diffractometer with Cu-Kα irradiation (λ=0.154178 nm) at 40 kV and 40 mA. The morphology of the samples was investigated with field emission scanning electron microscopy (FESEM) by JSM-6700F microscope. The high-resolution transmission electron microscope (HRTEM) observation was conducted using a LaB_6 JEM-2100 electron microscope. X-ray photoelectron spectroscopy (XPS) measurement was performed on a Kratos XSAM 800

* Corresponding author. Tel./fax: +86 27 8394 3956.
E-mail address: willycb@163.com (B. Chai).

0167-577X/$ - see front matter © 2012 Elsevier B.V. All rights reserved.
http://dx.doi.org/10.1016/j.matlet.2012.10.132

with Mg-Kα source operation at 200 W. The UV–vis diffuse reflectance spectra (DRS) were obtained by a Shimadzu UV-3600 spectrophotometer equipped with an integrating sphere using $BaSO_4$ as the reference sample. The BET surface areas were analyzed by nitrogen adsorption at 77 K with a Micromeritics ASAP 2020 nitrogen adsorption apparatus.

3. Results and discussion

Fig. 1 shows the XRD patterns of two representative samples synthesized by altering PVP adding amount. As shown in Fig. 1a, the diffraction peaks of obtained product without PVP can be ascribed to the rhombohedral CuSCN (JCPDS, No. 73-1855), which is in agreement with the literature [22]. No diffraction peak for any other crystal phase is detected, indicating that there is no crystal phase impurity existing in the obtained sample. The diffraction peaks at 2θ values of 16.2, 27.4, 32.8, 34.8, 47.3 and 50.3° can be attributed to the reflection of (006), (012), (0012), (018), (110) and (116) planes of the rhombohedral CuSCN, respectively. The broadening of diffraction peak in the sample prepared with PVP indicates the crystallite size decrease. In addition, the intensity of (012) plane is obviously weaker than that of sample prepared without PVP. This implies that the CuSCN growing along the (012) plane has been inhibited.

The representative SEM and TEM images of CuSCN products are shown in Fig. 2a–d. As can be seen from Fig. 2a, the CuSCN sample synthesized without PVP presents irregular particles together with some polyhedral products. Fig. 2b shows the uniform CuSCN spheres prepared with PVP of the average diameter about 0.5–0.6 μm. The spheres are comprised of much smaller nanoparticles, which is consistent with XRD analysis. From the broken CuSCN spheres, it is also found that there is a smaller nanosphere in it. As a result, they exhibit a ball-in-ball hollow architecture. In this case, the PVP plays an important role in the formation of CuSCN products. The TEM image of CuSCN spheres in Fig. 2c further confirms the presence of ball-in-ball hollow structure. The outer spheres have a shell wall thickness of ca. 50 nm. The inner nanospheres with a diameter of about 60% of the outer one are also constituted with nanoparticles. As can be seen from the HRTEM image in Fig. 2d, the interplanar spacing is measured to be 0.328 nm, which agrees with the (012) plane of rhombohedral CuSCN.

The formation mechanism of CuSCN hollow spheres was investigated by the time-dependent evolution experiments [7,8]. Intermediate products were collected at different stages, and their morphologies were subjected to SEM investigation, as is shown in Fig. 3. Prior to adding KSCN solution, the sample is solid spheres with the diameter of 0.5–1 μm. The surfaces of the spheres are relatively smooth (Fig. 3a). When adding KSCN solution and keeping 5 min without stirring, the surfaces of the spheres become rougher, which contains nanosized crystalline particles (Fig. 3b). Extending the reaction time to 15 min, there are some broken spheres in the products (Fig. 3c). With further increasing the reaction time to 30 min, the samples present hollow spheres with nanoparticles aggregation structure in Fig. 3d.

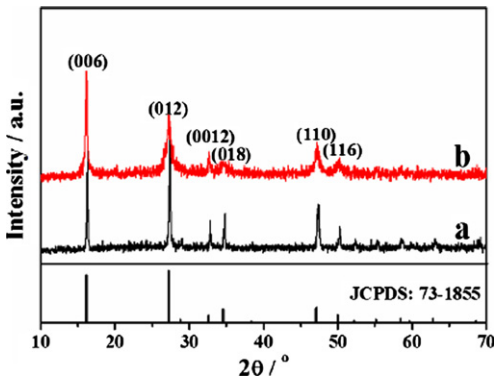

Fig. 1. XRD patterns of CuSCN samples prepared without (a) and with (b) PVP.

On the basis of the above evolution experiments of time-dependent morphology, it is believed that the difference of solubility products (K_{sp}) of CuBr (4.15×10^{-8}) and CuSCN (4.8×10^{-15}) or chemical self-transformation should be the main driving forces for the formation of these hollow spheres [7–13]. Initially, the PVP molecules were absorbed on the surface of CuBr crystalline particles when PVP were added into the mixture solution. Driven by the minimization of the total surface energy of the system, the CuBr particles can be self-assembled into spheres. As the KSCN solution is added to the suspension of CuBr, CuSCN preferentially deposits on the surface of CuBr spheres by heterogonous nucleation, resulting in the formation of nanosized CuSCN particle on the surface of CuBr. The inner CuBr core remains out of equilibrium and has a strong tendency to dissolve due to the reduction of the Cu^+ concentration in the solution. In this case, Br^- ions from the dissolved CuBr core will diffuse outward, while SCN^- ions in the solution diffuse inward. The PVP molecules adsorbed the surface of CuBr, which restrained the SCN^- ions inward diffusion rate. One the other hand, the diffusion rate of Br^- ions is obviously faster than that of SCN^- ions due to the former having smaller radii. As a result, the inward growth rate of CuSCN particle is slower than the dissolution rate of CuBr, the ball-in-ball CuSCN has been formed with hollow interior structure.

Fig. 4a displays the XPS survey spectrum for CuSCN sample prepared with PVP. As expected, it contains Cu, S, C and N elements. The high-resolution Cu 2p spectrum is shown in Fig. 4b, the peaks at 932.3 eV (Cu $2p_{3/2}$) and 952.2 eV (Cu $2p_{1/2}$) reveal that the oxidation state of Cu in the products is +1 rather than +2 [23]. The C 1s XPS spectrum is illustrated in Fig. 4c, which can be deconvoluted as two peaks. The peaks located at 284.8 and 285.7 eV are ascribed to adventitious carbon and C≡N bonds, respectively [14]. The N 1s peak (Fig. 3d) has a binding energy at 398.3 eV, consistent with C≡N bonds [14].

Fig. 5a shows the comparison of UV–vis diffuse reflectance absorption spectra (DRS) of CuSCN samples prepared with or without PVP. A significant increase in the absorption at wavelengths ca. 350 nm can be attributed to the intrinsic band-gap absorption of CuSCN. It is obvious that the CuSCN sample prepared with PVP presents a clear blue shift in the bandgap transition. The shift of the absorption edge toward shorter wavelengths indicates an increase in the bandgap energy of CuSCN, which is caused by strengthening of the quantum confinement of charge carriers in smaller CuSCN nanocrystalline particles. Assuming a direct band gap, the absorption data were then plotted as $(\alpha h\nu)^2$ versus photon energy (α=absorbance coefficient, h=Planck's constant, and ν=frequency), and the linear region of the onset of absorption was extrapolated to zero, as shown in the inset of Fig. 5a. The bandgap energies are 3.74 and 3.77 eV for the CuSCN samples obtained without and with PVP, respectively.

Fig. 5b depicts a representative N_2 adsorption–desorption isotherm and pore size distribution for the ball-in-ball CuSCN hollow structure. The isotherm can be categorized as type IV with H3 hysteresis loop, which is characteristic of mesoporous materials. The BET specific surface area of the sample was calculated to be 30.5 m^2/g. The powder has a bimodal pore size distribution with diameter 8–9 nm and 14–15 nm, determined by using the Barret–Joyner–Halenda (BJH) method (inset in Fig. 5b). The bimodal pore size distribution results from two different